Structures of [001] twist boundaries in gold. I. Measurement and use of absolute boundary x-ray structure factors

M. S. Taylor, I. Majid, P. D. Bristowe, and R. W. Balluffi
Department of Materials Science and Engineering, Massachusetts Institute of Technology, Cambridge, Massachusetts 02139
(Received 21 November 1988)

An x-ray-diffraction method for measuring absolute grain-boundary structure factors is described. The method is based on ratioing appropriate integrated scattered intensities from the grain-boundary region and from the adjoining perfect-crystal region in a bicrystal specimen containing a flat grain boundary. Common unknown factors then cancel out, and an expression for the absolute structure factor is obtained in which all quantities are either known, can be measured, or can be calculated with acceptable accuracy. A practical experimental technique for making the necessary measurements, which employs a four-circle diffractometer, is described. The technique is applied to an x-ray diffraction study of the atomistic structures of a series of [001] twist boundaries in gold in the following paper of our work. The results obtained there clearly demonstrate that the measurement of absolute structure factors, rather than relative structure factors, provides important information in diffraction studies of the structures of grain boundaries, particularly in cases where a limited number of structure factors is measured.

I. INTRODUCTION

X-ray diffraction has recently emerged as a technique with which to study the atomistic structure of grain boundaries.[1–8] Thin-film bicrystal specimens in the layered configuration shown in Fig. 1 have been employed. The atoms in the relatively thin boundary region are generally displaced with respect to the positions they would occupy in ideally perfect crystals 1 and 2 and, hence, produce an extra scattering that would not be present if they were an ideal lattice positions. Such boundary scattering is quite weak because of the relatively small number of atoms that are significantly displaced, and tends to be peaked on the so-called "boundary diffraction lattice" (or BDL),[9] which is described in Sec. II. This scattering is generally measured and then compared with corresponding scattering calculated for various atomistic models of the boundary structure in efforts to obtain structures yielding self-consistency.

Essentially all of the experimental effort in this field has focused on a number of [001] twist boundaries in gold. The published work[1–8] has consisted of the measurement of relative diffracted "intensities" on the BDL of these boundaries, and the comparison of these results with corresponding calculated boundary structure factors for various boundary models. The earlier work[1–5] must be regarded as essentially qualitative, since the precise relationship between the measured relative "intensities" and the boundary structure factors was not defined. Very recently, however, Fitzsimmons and Sass,[7,8] following Warren[10] and Robinson,[11] have developed a diffractometer technique which measures well-defined grain-boundary integrated intensities and corresponding structure factors on a relative basis and have applied the technique to determining the structures of the $\Sigma 5^7$ and $\Sigma 13^8$ [001] twist boundaries in gold. However, the atomistic structure of the $\Sigma 5$ boundary deduced in this work possesses atomic displacements which are considerably larger than those predicted by any reasonable physical model based on empirical pair potentials[4] or the "embedded-atom model" formulation.[12,13] This result has been surprising to workers in the field and has cast some doubt on the usefulness of the pair-potential and embedded-atom models.

A drawback of much of the diffraction work to date is that only relative structure factors have been measured experimentally for a limited number of reflections per boundary. These quantities have been measured in arbitrary units, and a normalizing scale factor has then been introduced in order to allow comparison with corresponding values calculated for models of the boundary structure. The scale factor has been determined by requiring agreement between measured and calculated values for one (or one pair) of relatively strong boundary reflections. It is easily seen, however, that important information regarding the atomic displacements can be

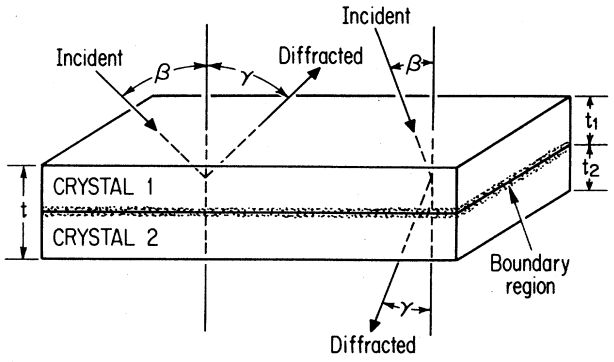

FIG. 1. Thin-film bicrystal specimen showing geometry of diffraction in both reflection (on left) and transmission (on right) modes.

missed when such a normalizing procedure is used. Many calculations have shown that the intensity of the boundary scattering depends sensitively on the magnitudes of the atomic displacements in the boundary, as might be expected. This information is lost when only relative measurements of the scattered intensity (and structure factors) are made. Erroneous results can, therefore, be obtained, particularly in situations where only a limited number of structure factors have been measured, as has been the case for boundary studies where the scattering is weak and difficult to measure.

In view of this situation, we have developed a diffractometer technique that allows the quantitative experimental measurement of absolute grain-boundary structure factors. The technique is relatively straightforward and avoids the need for determining the resolution function of the particular experimental arrangement. In the present work (paper I), we describe the technique and the analysis on which it is based, and also give a brief account of the way it can be used to gain information about grain-boundary structures by utilizing x-ray diffraction and computer simulation. In paper II,[14] we apply the method to the investigation of the structures of the series of [001] twist boundaries in gold, which includes the $\Sigma 113$, $\Sigma 25$, $\Sigma 13$, $\Sigma 17$, and $\Sigma 5$ boundaries. Good agreement is obtained for all boundaries between experimentally measured absolute structure factors and corresponding structure factors of boundary structures calculated by computer simulation using the embedded-atom model. The structure of the $\Sigma 5$ boundary, determined by Fitzsimmons and Sass,[7] is shown to possess displacements that are much too large, and, hence, it is incorrect. These results lead to the important conclusion that the atomistic structures calculated by means of the embedded-atom model are realistic, and, hence, lend credence to this method of calculating boundary structure.

II. THE BOUNDARY DIFFRACTION LATTICE (BDL)

We are concerned with a specimen of the form shown in Fig. 1, containing a boundary with a two-dimensional (2D) structure corresponding to the periodicity of the coincidence site lattice (CSL) parallel to the boundary. The thicknesses of crystals 1 and 2 are larger than the thicknesses of the boundary region in each crystal, defined as the regions where significant atom displacements are present. Such a specimen can be regarded as a 2D "crystal" composed of the unit cells shown in Fig. 2, where $\mathbf{a}_1$ and $\mathbf{a}_2$ define the 2D periodicity in the boundary plane, and $\mathbf{t}$ is a vector normal to the surface and of magnitude equal to the total specimen thickness. The diffracted intensity is then expected to fall on a lattice in reciprocal space, i.e., the BDL, composed of an array of line elements that, as shown in Fig. 3, run perpendicular to the boundary and project on the boundary plane in a pattern corresponding to the reciprocal lattice of the 2D boundary lattice defined by $\mathbf{a}_1$ and $\mathbf{a}_2$.[9] The unit vectors of the BDL are taken to be $\mathbf{a}_1^*$, $\mathbf{a}_2^*$, and $\mathbf{k}$. The vector $\mathbf{k}$ is parallel to $\mathbf{t}$, and a convenient choice for its magnitude is the smaller of the spacings of the planes in the reciprocal lattices of crystals 1 and 2, which lie parallel to the boundary. A general vector in this space is represented by

$$\mathbf{g}=H\mathbf{a}_1^*+K\mathbf{a}_2^*+L\mathbf{k} .$$

All lattice reflections from the perfect crystals 1 and 2 fall on a subset of the elements of the BDL. The additional scattered intensity due to the displaced atoms in the boundary region falls, more generally, on elements of the BDL in the form of patches corresponding to relrods (reciprocal-lattice rods shown schematically in Fig. 3), which are elongated along L because of the relatively small thickness of the boundary region.

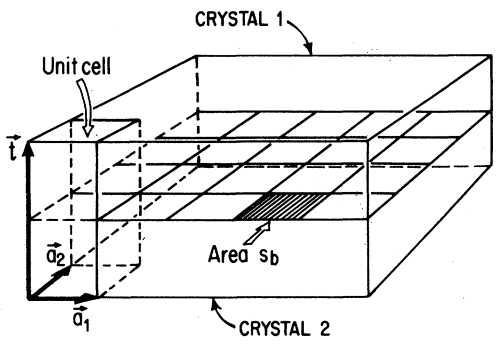

FIG. 2. Unit cells for boundary structure.

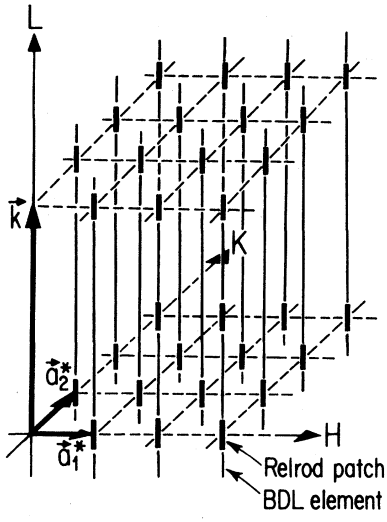

FIG. 3. Boundary diffraction lattice (BDL). The base vectors, $\mathbf{a}_1^*$ and $\mathbf{a}_2^*$, are reciprocal to $\mathbf{a}_1$ and $\mathbf{a}_2$ in Fig. 2, and $\mathbf{k}$ is perpendicular to the boundary. Relrods of diffracted intensity from the boundary are present on the BDL line elements, as shown schematically.

III. ANALYSIS FOR ABSOLUTE GRAIN-BOUNDARY STRUCTURE FACTORS

We assume that the specimen, consisting of a 2D assemblage of unit cells as in Fig. 2, has the shape of a parallelogram with sides equal to $N_1\mathbf{a}_1$ and $N_2\mathbf{a}_2$. Diffraction can be in reflection or transmission modes, as

illustrated in Fig. 1. Using standard methods and assuming simple kinematic scattering,[10] the scattered intensity at a distance R is then

$$J = I_0 \left[\frac{e^4}{m^2 c^4 R^2} \right] \frac{\sin^2(\pi N_1 H)}{\sin^2(\pi H)} \frac{\sin^2(\pi N_2 K)}{\sin^2(\pi K)} f_b^2 |F_b|^2 B_b \ , \tag{1}$$

where I_0 is the incident-beam intensity, e the electron charge, m the electron mass, c the velocity of light, f_b the atomic-scattering factor, $F_b = F_b(H,K,L)$ the "reduced" structure factor of the unit cell (assuming unity as the scattering factor of each atom), and B_b the polarization factor, given by

$$B_b = \frac{1 + (\cos^2 2\theta_m)(\cos^2 2\theta_b)}{1 + \cos^2 2\theta_m} \ . \tag{2}$$

Here, θ_m is the Bragg-scattering angle for the monochromator used in the present experimental technique (see Sec. IV A), and θ_b is the usual scattering angle. If the Bragg condition was satisfied exactly, Eq. (1) would give a peak intensity of

$$J = I_0 \left[\frac{e^4}{m^2 c^4 R^2} \right] N_1^2 N_2^2 f_b^2 |F_b|^2 B_b \ . \tag{3}$$

As in the case of 3D crystallography, however, Eq. (3) does not represent a measurable quantity. Instead, we turn to the notion of an integrated intensity, which can be both calculated and measured. Such an integrated intensity is the total-energy flow (i.e., power), which is diffracted when the Ewald sphere intersects a relrod on the BDL, as illustrated in Fig. 4. In this situation, the specimen is held in fixed position, and the total counting rate produced by the intersection of the Ewald sphere with the relrod is counted as indicated schematically.

The contribution to the total power, $\dot{E}_b$, diffracted by the grain boundary from a patch of area dA lying on the intersection of the Ewald sphere with the relrod is

$$d\dot{E}_b = R^2 \lambda^2 J \, dA \ , \tag{4}$$

where λ is the x-ray wavelength. Now,

$$dA = \frac{\mathbf{a}_1^* dH \cdot \mathbf{a}_2^* dK}{\cos\gamma_b} = \frac{dH \, dK}{s_b \cos\gamma_b} \ , \tag{5}$$

where s_b is the area of the unit-cell face in the grain boundary, and γ_b is the angle between the grain-boundary normal and the diffracted beam. Inserting Eqs. (3) and (5) into Eq. (4), we can neglect the relatively slow variation of $F_b(H,K,L)$ with H, K, and L, and integrate over the entire intersection with the relrod to obtain

$$\dot{E}_b = I_0 \left[\frac{e^4}{m^2 c^4} \right] \frac{\lambda^2 B_b f_b^2 |F_b(H,K,L)|^2 N_1 N_2}{s_b \cos\gamma_b} \ . \tag{6}$$

Setting n_b equal to the number of unit cells per unit area of grain boundary in real space, we have

$$\frac{N_1 N_2}{s_b} = n_b^2 S_b \ , \tag{7}$$

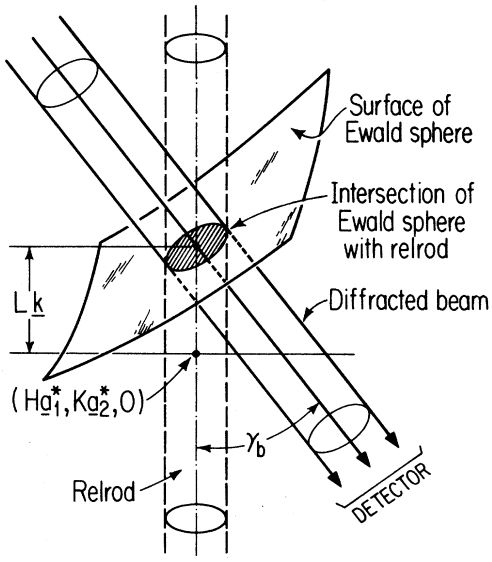

FIG. 4. Intersection of Ewald sphere with grain-boundary intensity relrod. Intersection located on BDL at $(H\mathbf{a}_1^*, K\mathbf{a}_2^*, L\mathbf{k})$.

where S_b is the total area of grain boundary irradiated. Therefore,

$$\dot{E}_b = I_0 \left[\frac{e^4}{m^2 c^4} \right] \lambda^2 B_b f_b^2 |F_b(H,K,L)|^2 \frac{n_b^2 S_b}{\cos\gamma_b} \ . \tag{8}$$

So far, we have not corrected for energy losses due to mass absorption in crystals 1 and 2. If β_b is the angle between the incident beam and the boundary normal, the diffracted radiation follows a total path length in the specimen given by

$$l_b = t_1 / \cos\beta_b + t_2 / \cos\gamma_b \tag{9a}$$

for the transmission case, and

$$l_b = t_1 / \cos\beta_b + t_1 / \cos\gamma_b \tag{9b}$$

for the reflection case, where t_1 is the thickness of crystal 1 (assumed to be on the incident side, as in Fig. 1) and t_2 is the thickness of crystal 2. Therefore, finally,

$$\dot{E}_b = P_0 \left[\frac{e^4}{m^2 c^4} \right] \lambda^2 B_b f_b^2 |F_b(H,K,L)|^2 \times \exp(-\mu l_b) \frac{n_b^2}{(\cos\gamma_b)(\cos\beta_b)} \ , \tag{10}$$

where P_0 is the total power of the beam incident on the specimen, and μ is the linear absorption coefficient.

At this point, it is worth noting the differences between measuring an integrated intensity in two dimensions and in three dimensions. In the 3D case, i.e., in a lattice reflection, the integration is carried out in two steps: First, one integrates over the entire receiving area, and then over all incident-beam directions. Experimentally, the first integration is carried out by setting the receiving counter slit so wide that all of the diffracted radiation is recorded, while the second integration involves rotating

the crystal through the Bragg reflection. In this way, all parts of the crystal satisfy Bragg's law with each element of the primary beam. In the 2D case, however, only the integration over the receiving surface is necessary. The integration over all incident-beam directions is done automatically, since the reciprocal-space intensity distribution involves relrods and not points. Experimentally, then, one must still use a receiving slit that is wide enough to collect all of the diffracted intensity, but in the 2D case the crystal need not be rotated.

In principle, absolute values of $|F_b(H,K,L)|$ could be calculated from Eq. (10) if all other factors were known. However, the quantity P_0 is difficult to determine. We therefore adopt a procedure in which we normalize the integrated grain-boundary intensity to the integrated intensity from a crystal-1 or crystal-2 reflection that is nearby in reciprocal space. Using standard methods again,[10] the total energy scattered by either crystal 1 or 2 in Fig. 1, when the Ewald sphere is passed through one of its Bragg reflections by rotations at a rate $\dot{\omega}$, is

$$E_c=\frac{P_0}{\dot{\omega}}\left[\frac{e^4}{m^2c^4}\right]\lambda^3 B_c f_c^2|F_c(H,K,L)|^2\frac{n_c^2 A_c}{(\sin 2\theta_c)(\cos\beta_c)}\ , \tag{11}$$

where the subscript c indicates crystal quantities, and the quantity A_c for the transmission case is given by

$$A_c=\begin{cases}\dfrac{\exp(-\mu t/\cos\gamma_c)\{1-\exp[-\mu t_1(1/\cos\beta_c-1/\cos\gamma_c)]\}}{\mu(1/\cos\beta_c-1/\cos\gamma_c)} & \text{(for crystal 1 excited)}\ ,\\ \dfrac{\exp(-\mu t/\cos\beta_c)\{\exp[\mu t_2(1/\cos\beta_c-1/\cos\gamma_c)]-1\}}{\mu(1/\cos\beta_c-1/\cos\gamma_c)} & \text{(for crystal 2 excited)}\ ,\end{cases} \tag{12a}$$

and for the reflection case by

$$A_c=\begin{cases}\dfrac{1-\exp[-\mu t_1(1/\cos\beta_c+1/\cos\gamma_c)]}{\mu(1/\cos\beta_c+1/\cos\gamma_c)} & \text{(for crystal 1 excited)}\ ,\\ \dfrac{\exp[-\mu t_1(1/\cos\beta_c+1/\cos\gamma_c)]-\exp[-\mu t(1/\cos\beta_c+1/\cos\gamma_c)]}{\mu(1/\cos\beta_c+1/\cos\gamma_c)} & \text{(for crystal 2 excited)}\ .\end{cases} \tag{12b}$$

Here, β_c and γ_c are the angles made by the incident and scattered beams with the boundary normal, and we have again assumed that crystal 1 is on the incident side, as in Fig. 1. Also,

$$B_c=\frac{1+(\cos^2 2\theta_m)(\cos^2 2\theta_c)}{1+\cos^2 2\theta_m}\ . \tag{13}$$

Under conditions in which the incident beam is maintained constant, and where the incident power delivered to both the grain-boundary region and either crystal 1 or crystal 2 is the same, the P_0 terms in Eqs. (10) and (11) cancel. In addition

$$\dot{C}_b=K\dot{E}_b\ , \tag{14}$$

$$C_c=KE_c\ , \tag{15}$$

where $\dot{C}_b$ is measured x-ray counting rate in the boundary experiment, C_c is measured number of counts in the crystal experiment, and K is a constant of proportionality. Finally, by combining Eqs. (10) and (11) and using Eqs. (14) and (15), we obtain

$$\frac{|F_b(H,K,L)|^2}{|F_c(H,K,L)|^2}=\left[\frac{\dot{C}_b}{C_c\dot{\omega}}\right]\left[\frac{B_c}{B_b}\right]\left[\frac{f_c^2}{f_b^2}\right]\frac{1}{\exp(-\mu l_b)}\left[\frac{n_c^2 A_c\lambda}{n_b^2}\right]\left[\frac{(\cos\gamma_b)(\cos\beta_b)}{(\sin 2\theta_c)(\cos\beta_c)}\right]\ . \tag{16}$$

All quantities on the right-hand side of Eq. (16) are either known, can be measured, or can be calculated. Since $|F_b|^2$ and $|F_c|^2$ are functions of temperature, the experiment, therefore, yields the ratio $|F_b|^2/|F_c|^2$ at the temperature of measurement. If the experiment is carried out at room temperature (as is commonly the case), the best procedure would be to use a molecular-dynamics model to calculate $|F_c|^2$ at room temperature. Absolute values of $|F_b|^2$ could then be obtained from Eq. (16), which could then be compared with grain-boundary structure factors for boundary models also calculated by the same molecular-dynamics model at the same temperature.

On the other hand, if molecular-dynamics models are unavailable, the known static values of $|F_c|^2$ corresponding to the perfect crystal without thermal vibration can

be used in Eq. (16), along with a relatively small Debye-Waller correction factor in order to obtain corresponding static values of $|F_b|^2$ (designated in the following by $|F_b^0|^2$), which can be compared with calculated values of $|F_b^0|^2$ using molecular statics modeling. In this procedure, the effects of temperature in modifying the structure factors are eliminated to a considerable extent because $|F_b|^2$ and $|F_c|^2$ appear as a ratio. In fact, the only temperature effect that arises is that due to the difference between the Debye-Waller factor for the grain boundary and that for the lattice, and we therefore have

$$|F_b^0|^2=\frac{|F_b|^2}{|F_c|^2}|F_c^0|^2\Gamma\ , \tag{17}$$

where the experimentally determined ratio $|F_b|^2/|F_c|^2$ is given by Eq. (16), $|F_c^0|^2=16$ for the case of gold, and the correction factor Γ, due to the difference between Debye-Waller factors, is given by

$$\Gamma=\exp\left[\frac{16\pi^2}{\lambda^2}(\langle u_b^2\rangle\sin^2\theta_b-\langle u_c^2\rangle\sin^2\theta_c)\right]\ , \tag{18}$$

where $\langle u_b^2\rangle$ and $\langle u_c^2\rangle$ are the mean-square displacements of atoms projected along the diffraction vector[10] in the grain boundary and in the perfect crystal, respectively. As shown in paper II,[14] the correction factor Γ is close to unity and can be estimated to a degree of accuracy sufficient for present purposes.

IV. EXPERIMENTAL TECHNIQUE

A. Diffractometer and specimen

Since the boundary scattering is relatively weak and also has a complicated distribution in reciprocal space, a special diffractometer was constructed. In general, the instrument consisted of an 18-kW rotating-anode x-ray source, monochromating and collimating optics, a precision four-circle goniometer, and two x-ray scintillation detectors in the arrangement illustrated in Fig. 5. Most of the beamline path was under vacuum. The system was fully computer controlled with automated data acquisition. Features were also added which allowed the convenient measurement of the bicrystal specimen

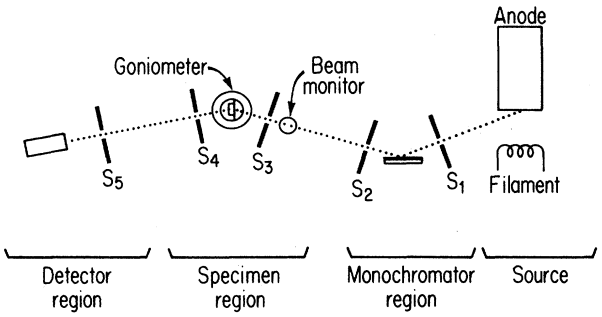

FIG. 5. General top-view arrangement of diffractometer.

geometry. In the following, we give a brief description of the equipment. Further details may be found in Ref. 15.

The optics of the incident beam (Cu $K\alpha$ radiation) were controlled by the collimating slits and the monochromator. The monochromator was a singly bent, graphite single crystal with is cylindrical axis parallel to the scattering plane, which was placed so that it focused the incident beam approximately at the specimen. The beam intensity was automatically monitored by a detector which received x rays that were scattered at right angles to the beamline path by a thin Kapton polymer film intersecting the beam.

The four-circle goniometer was a standard Huber instrument with the ϕ, χ, ω, and θ axes illustrated in Fig. 6. It was driven by four stepping motors that were controlled by a slightly modified computer program originally written by Professor Mark Sutton of McGill University for use on the MIT/IBM beamlines at the Brookhaven synchrotron. The program also collected and stored data and allowed one to work in either real or reciprocal space by scanning in terms of angles or in terms of the reciprocal lattice of either crystal 1 or crystal 2.

The specimen possessed the geometry shown in Fig. 1, which had the advantage that a relatively large ratio of grain-boundary "volume" to perfect-crystal volume could be achieved by using a specimen of small thickness. This was important in reducing the background scattering produced by the two perfect-crystal regions. In addition, the parallel crystal geometry allowed accurate correction for absorption effects, Eqs. (12a) and (12b). The actual specimens used were 75 nm thick and $\sim$5 mm$\times$5 mm in lateral dimensions, and were mounted flat on 7.6-μm-thick Kapton polymer films, which, in turn, were stretched on aluminum ring-shaped holders in the configuration shown in Fig. 7. Great care was taken to avoid wrinkling and to obtain as flat a specimen as possible [see paper II (Ref. 14) for preparation details]. This ensemble was then mounted on the ϕ axis of the goniometer (Fig. 6), so that the center of the specimen coincided with the center of rotation of the gonimeter. Finally, the optics of the diffracted beam and detector system were controlled by the collimating slits shown in Fig. 5.

The diffractometer technique also included several features which greatly aided in the determination of the geometry of the bicrystal specimen. In order to determine the misorientation of crystals 1 and 2, the diffractometer recorded the angular settings required to excite two well-separated Bragg reflections in each crystal. The twist and tilt misorientations (in terms of the misorientations around an axis normal to the boundary plane and the tilt misorientation around an axis lying in the boundary plane, respectively) were then automatically calculated. The orientations of the boundary plane relative to the crystal axes of crystals 1 and 2 were obtained by a laser-reflection technique. In the present specimens, the grain boundary was very accurately parallel to the specimen surfaces. By reflecting the beam from the laser shown in Fig. 6 off the specimen and back on itself, and reading the corresponding diffractometer angles, the necessary information was obtained to allow the automatic calculations of these orientations.

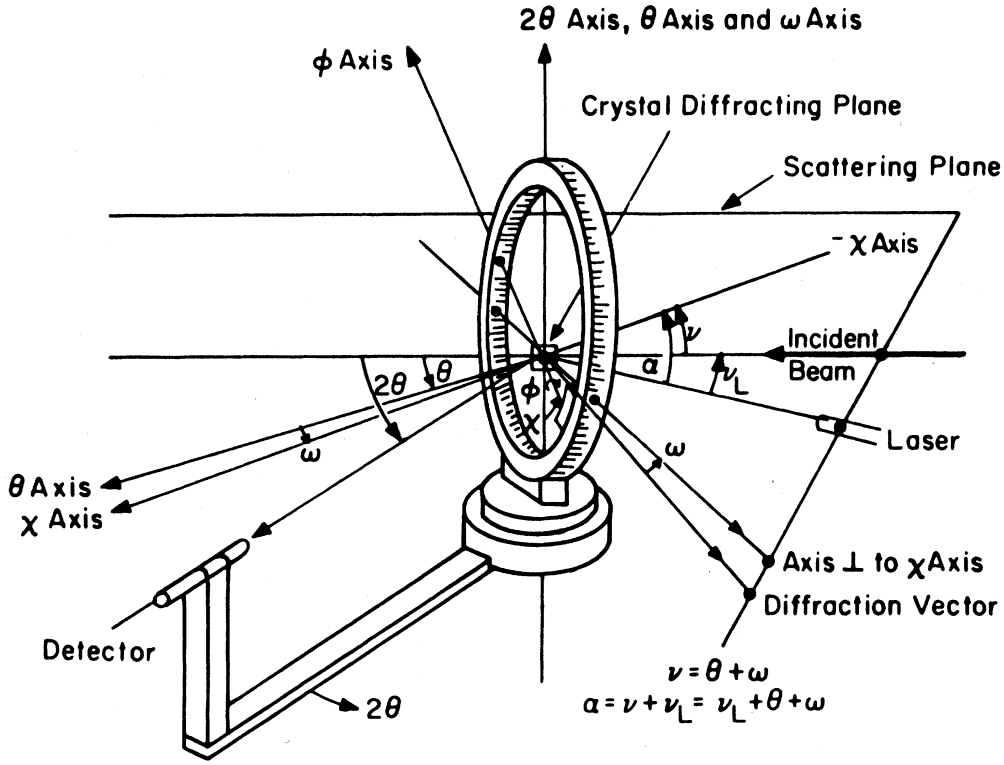

FIG. 6. Four-circle goniometer. Also shown are detector and laser.

B. Operating details

Because of the weakness of the grain-boundary scattering, the diffractometer was run with relatively large apertures and divergent beams in a low-resolution mode in an effort to increase the counting rates. However, this tended to decrease the signal-to-background ratio and, also, of course, the resolution, and it was therefore necessary to strike a compromise with regard to these factors.

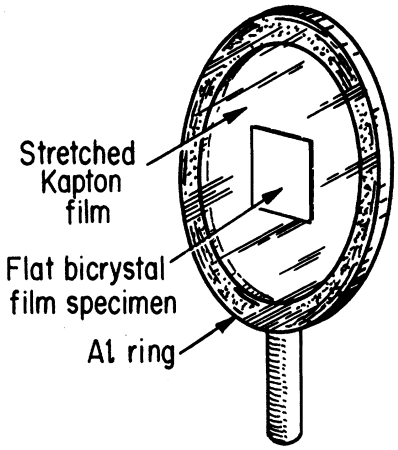

FIG. 7. Flat bicrystal specimen mounted on Kapton film, which, in turn, is stretched on aluminum ring that mounts on the gonimeter.

The incident-beam optics, particularly the openings in slit S_3 in Fig. 5, were made large enough to ensure that all of the desired radiation from the monochromator was incident on the sample. Typical divergences in the horizontal plane were $\sim 0.4°$, and a value somewhat larger in the vertical direction due to the focusing action of the bent monochromator. The detector optics were adjusted to minimize the inciden-beam path length "seen" by the detector. This tended to improve the signal-to-background characteristics of the arrangement. The actual background in a scan was, of course, a strong function of position in reciprocal space, being dominated by thermal diffuse scattering from the specimen when close to the crystal lattice reflections (e.g., in the case of low-angle twist boundaries), and dominated by air and Kapton scattering when much further away (as in the case of high-angle twist boundaries). Typical scans [e.g., see Fig. 3 of paper II (Ref. 14)] extended over about 5° in 2θ in intervals of 0.3°; counting times varied between 5 and 45 min per point, depending on the strength of the grain-boundary reflection.

Careful attention was paid to the proper measurement of the important quantities, $\dot{C}_b$ and C_c. The measurement of $\dot{C}_b$ required the measurement of *all* of the scattering produced by the intersection of the Ewald sphere and the grain-boundary relrod. Since the incident beam was significantly divergent, and since the specimen was bent to at least some degree, the scattered beam was relatively broad at the detector, and care had to be taken to count all of the radiation. This was accomplished by

increasing the vertical acceptance of the detector system to the required level, and moving the detector through the grain-boundary peak horizontally (in a 2θ scan) in increments equal to its acceptance aperture. In this way, erroneous values of $\dot{C}_b$ due to double counting were avoided. Similarly, C_c was obtained by rocking the sample over a large angular range, about 4°, around the exact Bragg angle, and collecting the entire diffracted beam by moving the detector in increments equal to its angular acceptance width.

ACKNOWLEDGMENTS

Support for one of us (M.S.T) was provided by the Center for Materials Science and Engineering (CMSE) at the Massachusetts Institute of Technology under U.S. National Science Foundation Grant No. PNDG-84-18718-DMR. Support for I.M., P.D.B., and R.W.B. was provided by the U. S. Department of Energy under Grant No. DE-FG02-E7ER-45310. We are grateful to the CMSE for the use of its Central X-ray Facility.

[1]S. L. Sass, J. Appl. Crystallogr. **13**, 109 (1980).
[2]S. L. Sass and P. D. Bristowe, in *Grain Boundary Structure and Kinetics,* edited by R. W. Balluffi (Amerian Society for Metals, Metals Park, OH, 1980), p. 71.
[3]J. Budai and S. L. Sass, J. de Phys. (Paris) Colloq. Suppl. 12, **43**, C6-103 (1982).
[4]J. Budai, P. D. Bristowe, and S. L. Sass, Acta Metall. **31**, 699 (1983).
[5]K. R. Milkove, P. Lamarre, F. Schmuckle, M. D. Vaudin, and S. L. Sass, J. Phys. (Paris) Colloq. Suppl. 4, **46**, C4-71 (1985).
[6]M. R. Fitzsimmons and S. L. Sass, in *Fundamentals of Diffusion Bonding,* edited by Y. Ishida (Elsevier, Amsterdam, 1987), p. 147.
[7]M. R. Fitzsimmons and S. L. Sass, Acta Metall. **36**, 3103 (1988).
[8]M. R. Fitzsimmons and S. L. Sass, Acta Metall. **37**, 1009 (1989).
[9]A. Brokman and R. W. Balluffi, Acta Metall. **31**, 1639 (1983).
[10]B. E. Warren, *X-Ray Diffraction* (Addison-Wesley, Reading, MA, 1969).
[11]I. K. Robinson, Aust. J. Phys. **41**, 359 (1988).
[12]M. S. Daw and M. I. Baskes, Phys. Rev. B **29**, 6443 (1984).
[13]P. D. Bristowe (unpublished).
[14]I. Majid, P. D. Bristowe and R. W. Balluffi, this issue, the following paper, Phys. Rev. B **40**, 2779 (1989).
[15]M. S. Taylor, Ph.D thesis, Massachusetts Institute of Technology, 1987.